Electronic Supplementary Information

"Tuning Aggregative versus Non-Aggregative Lectin Binding with Glycosylated Nanoparticles by the Nature of the Polymer Ligand"

*Panagiotis G. Georgiou,[a] Alexander N. Baker,[a] Sarah-Jane Richards,[a] Antonio Laezza,[a] Marc Walker,[c] and Matthew I. Gibson[a,b]**

[a] Department of Chemistry, University of Warwick, Gibbet Hill Road, CV4 7AL, Coventry, UK

[b] Warwick Medical School, University of Warwick, Gibbet Hill Road, CV4 7AL, Coventry, UK

[c] Department of Physics, University of Warwick, Gibbet Hill Road, CV4 7AL, Coventry, UK

**Corresponding Author*: m.i.gibson@warwick.ac.uk

Contents

Experimental Section

Materials and Methods

Materials

All chemicals were used as supplied unless otherwise stated. 1-Dodecanethiol (≥98%), 2-bromo-2-methylpropionic acid (98%), carbon disulfide (anhydrous, ≥99%), tripotassium phosphate (≥98%), pentafluorophenol (≥99%), 4-(dimethylamino)pyridine (≥98%, DMAP), *N*-(2-hydroxypropyl)methacrylamide (99%, HPMA), *N*-hydroxyethyl acrylamide (97%, HEA), triethylamine (>99%), sodium citrate tribasic dihydrate (>99%), gold(III) chloride trihydrate (99.9%), ammonium carbonate (reagent grade) were all purchased from Sigma-Aldrich. *N*-(3-dimethylaminopropyl)-*N*'-ethylcarbodiimide hydrochloride (EDC·HCl) was purchased from Carbosynth. D(+)-galactosamine hydrochloride (99%) was purchased from Acros Organics. Soybean agglutinin (SBA) lectin was purchased from Vector Laboratories. Clear and black half are 96-well plates were purchased from Greiner Bio-one. Streptavidin (SA) biosensors were purchased from Forte Bio. Lectin was biotinylated using EZ-Link Sulfo-NHS-LC-Biotin reagent from Thermo Fisher Scientific using standard procedure (20-fold molar excess of biotin reagent, conjugation performed in PBS buffer and isolated using Amicon Ultra-0.5 mL 3000 MWCO centrifugal filters from Merck Millipore). Gold nanoparticles of 20, 30 and 40 nm size were synthesized based on previously described process through seeded growth approach.[1] Photo-polymerization reactions were conducted using a blue LED strip light (3 meters with 180 LEDs) operating at a wavelength of λ = 460-465 nm. Formvar coated copper grids were purchased from EM Resolutions.

Characterization Techniques

NMR Spectroscopy. ^{1}H-NMR, ^{13}C-NMR and ^{19}F-NMR spectra were recorded at 300 MHz or 400 MHz on a Bruker DPX-300 or DPX-400 spectrometer respectively, with chloroform-*d* ($CDCl_3$) or methanol-d_4 (CD_3OD) as the solvent. Chemical shifts of protons are reported as δ in parts per million (ppm) and are relative to tetramethylsilane (TMS) at δ = 0 ppm when using $CDCl_3$ or solvent residual peak (CH_3OH, δ = 3.31 ppm).

FT-IR Spectroscopy. Fourier Transform-Infrared (FT-IR) spectroscopy measurements were carried out using an Agilent Cary 630 FT-IR spectrometer, in the range of 650 to 4000 cm^{-1}.

Size Exclusion Chromatography. Size exclusion chromatography (SEC) analysis was performed on an Agilent Infinity II MDS instrument equipped with differential refractive index (DRI), viscometry (VS), dual angle light scatter (LS) and variable wavelength UV detectors. The system was equipped with 2 x PLgel Mixed D columns (300 x 7.5 mm) and a PLgel 5 µm guard column. The mobile phase used was DMF (HPLC grade) containing 5 mM NH_4BF_4 at 50 °C at flow rate of 1.0 mL.min^{-1}. Poly(methyl methacrylate) (PMMA) standards (Agilent EasyVials) were used for calibration between 955,000 – 550 g.mol^{-1}. Analyte samples were filtered through a nylon membrane with 0.22 μm pore size before injection. Number average molecular weights (M_n), weight average molecular weights (M_w) and dispersities ($Đ_M = M_w/M_n$) were determined by conventional calibration and universal calibration using Agilent GPC/SEC software.

Dynamic Light Scattering. Hydrodynamic diameters (D_h) and size distributions of particles were determined by dynamic light scattering (DLS) using a Malvern Zetasizer Nano ZS with a 4 mW He-Ne 633 nm laser module operating at 25 °C. Measurements were carried out at an angle of 173° (back scattering), and results were analysed using Malvern DTS 7.03 software. All determinations were repeated 5 times with at least 10 measurements recorded for each run. D_h values were calculated using the Stokes-Einstein equation where particles are assumed to be spherical.

Zeta Potential Analysis. Zeta potential was measured by the technique of microelectrophoresis, using a Malvern Zetasizer Nano ZS instrument, at room temperature at 633 nm. All reported measurements were the average of at least five runs. Zeta potential was calculated from the corresponding electrophoretic mobilities (μ_E) by using the Henry's correction of the Smoluchowski equation ($\mu_E = 4\pi\,\varepsilon_0\,\varepsilon_r\,\zeta\,(1+\kappa r)/6\pi\,\mu$).

Transmission Electron Microscopy. Dry-state stained TEM imaging was performed on a JEOL JEM-2100Plus microscope operating at an acceleration voltage of 200 kV. All dry-state samples were diluted with deionized water and then deposited onto formvar-coated copper grids.

X-ray Photoelectron Spectroscopy. The x-ray photoelectron spectroscopy (XPS) data were collected at the Warwick Photoemission Facility, University of Warwick. The samples were attached to electrically-conductive carbon tape, mounted on to a sample bar and loaded in to a Kratos Axis Ultra DLD spectrometer which possesses a base pressure below 1 x 10^{-10} mbar.

XPS measurements were performed in the main analysis chamber, with the sample being illuminated using a monochromated Al Kα x-ray source. The measurements were conducted at room temperature and at a take-off angle of 90° with respect to the surface parallel. The core level spectra were recorded using a pass energy of 20 eV (resolution approx. 0.4 eV), from an analysis area of 300 μm x 700 μm. The spectrometer work function and binding energy scale of the spectrometer were calibrated using the Fermi edge and $3d_{5/2}$ peak recorded from a polycrystalline Ag sample prior to the commencement of the experiments. In order to prevent surface charging the surface was flooded with a beam of low energy electrons throughout the experiment and this necessitated recalibration of the binding energy scale. To achieve this, the C-C/C-H component of the C 1*s* spectrum was referenced to 285.0 eV. The data were analysed in the CasaXPS package, using Shirley backgrounds and mixed Gaussian-Lorentzian (Voigt) lineshapes. For compositional analysis, the analyser transmission function has been determined using clean metallic foils to determine the detection efficiency across the full binding energy range.

Methods

Saline stability-induced aggregation studies by absorbance. A solution of NaCl was made up ([NaCl] = 1M) followed by a 25 μL serial dilution in a clear, flat bottom, half area 96-well microtitre plate. 25 μL of the glyco-AuNP were added to each well and incubated at room temperature for 30 mins. After 30 minutes, an absorbance spectrum was recorded from 450 nm-700 nm with 10 nm intervals.

Lectin-induced aggregation studies by absorbance. A stock solution of the lectin (SBA) was made up (0.1 $mg.mL^{-1}$ and 1 $mg.mL^{-1}$ for PHEA and PHPMA-based glyco-AuNPs) in 10 mM HEPES buffer with 0.15 M NaCl, 0.1 mM $CaCl_2$ and 0.01 mM $MnCl_2$. 25 μL serial dilution was made up in the same buffer in a clear, flat bottom, half area 96-well microtitre plate. 25 μL of the glyco-AuNPs was added to each well and incubated at room temperature for 30 mins. After 30 minutes, an absorbance spectrum was recorded from 450 nm-700 nm with 10 nm intervals.

Biolayer interferometry. Biolayer Interferometry for Gal-$PHPMA_{36}$@Au40nm and Gal-$PHEA_{33}$@Au40nm was carried out on ForteBio Octet Red96 (Forte Bio, USA). Assays were performed in black 96 well half area plates. Assays were carried out at 30 °C and agitated at 1,000 rpm. Streptavidin (SA) biosensor tips (Forte Bio, USA) were hydrated in milliQ H_2O water for at least 10 mins prior to use. A stable baseline was established in milliQ water for 1

minute. The biosensors were functionalized by loading with 10 µg/mL biotinylated SBA in PBS for 5 mins followed by a 1-minute equilibration step in 10 mM HEPES with 0.15 M NaCl, 0.1 mM $CaCl_2$ and $MnCl_2$ to remove and unbound protein and to establish a stable baseline. Following protein immobilization, the binding association with galactosylated AuNPs was carried out in 10 mM HEPES with 0.15 M NaCl, 0.1 mM $CaCl_2$ and $MnCl_2$, for 10 minutes followed by dissociation in 10 mM HEPES with 0.15 M NaCl, 0.1 mM $CaCl_2$ and $MnCl_2$ for 10 minutes.

Supplementary Characterization Data for PFP-PHPMA/PHEA and Galactosamine-Functionalized Homopolymers

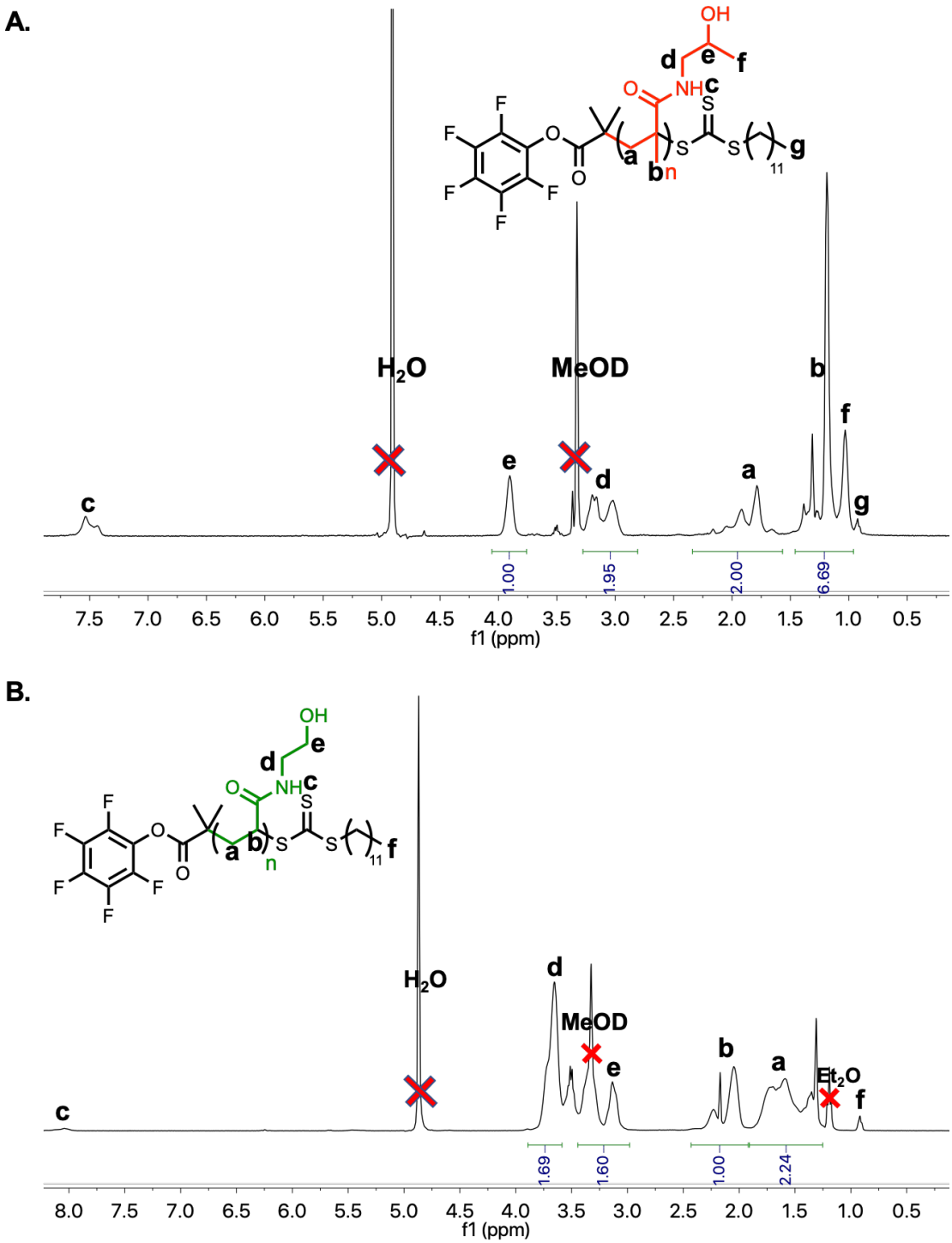

Figure S1. ^{1}H-NMR spectra of PFP-PHPMA$_n$ (A) and PFP-PHEA$_n$ (B) (n = 25, 33 respectively) homopolymers recorded in methanol-d_4.

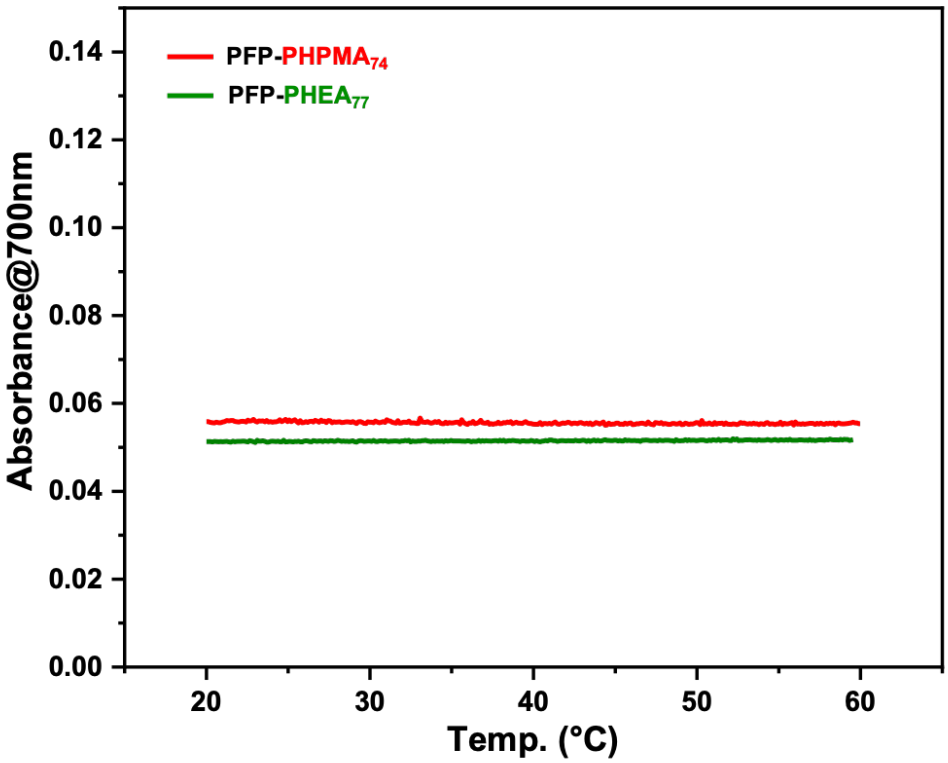

Figure S2. Turbidity curves upon heating of 10 mg.ml^{-1} solution of polymer PFP-PHPMA$_{74}$ and PFP-PHEA$_{77}$ in PBS at a heating rate of 1 °C min^{-1}.

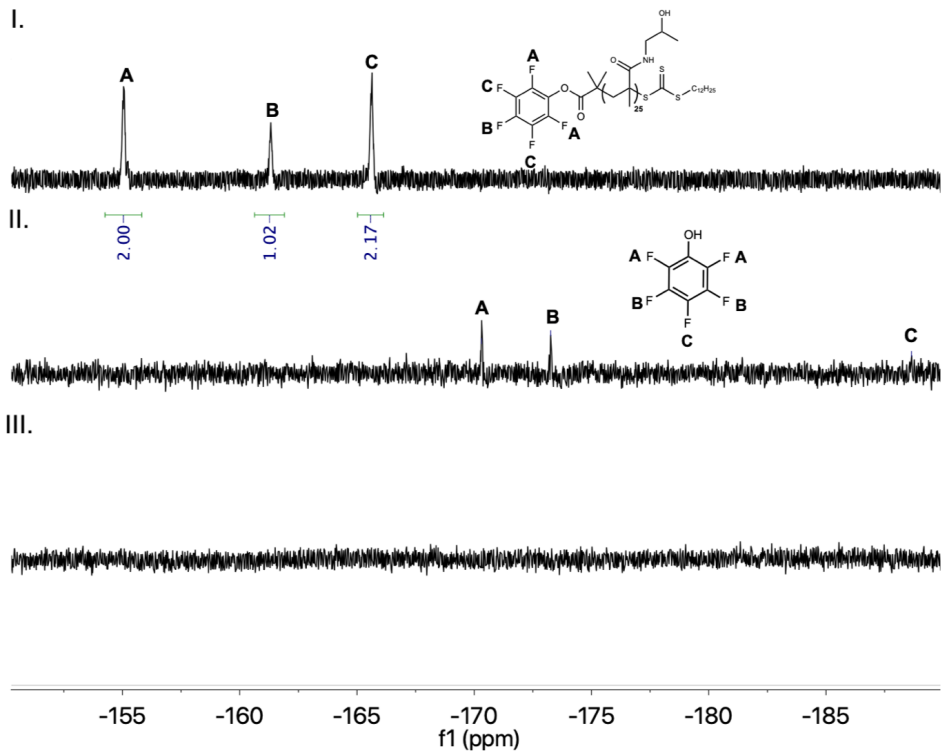

Figure S3. (I) ^{19}F NMR spectra for the purified PFP-PHPMA$_{25}$ homopolymer, (II) crude reaction of the polymer after post-functionalization with galactosamine, (III) purified galactosamine-functionalized polymer obtained after precipitation in diethyl ether. All spectra were recorded in methanol-d_4.

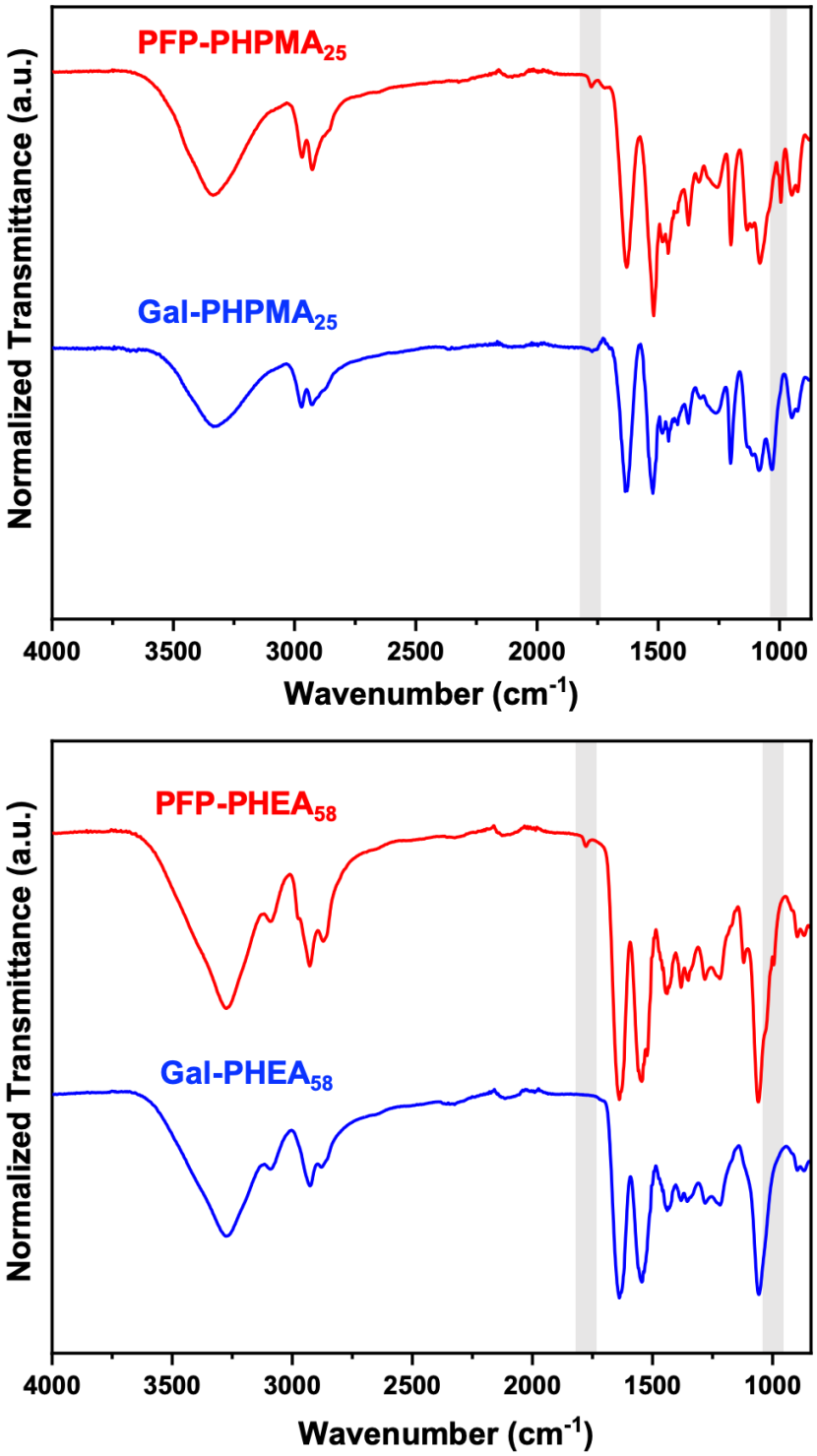

Figure S4. FT-IR spectra recorded for PHPMA and PHEA homopolymers before (red) and after (blue) end group modification with galactosamine showing the disappearance of the characteristic vibration peaks of PFP group at 950 and 1750 cm^{-1}.

Supplementary Characterization Data for Gal-PHPMA/PHEA-Coated Au-NPs

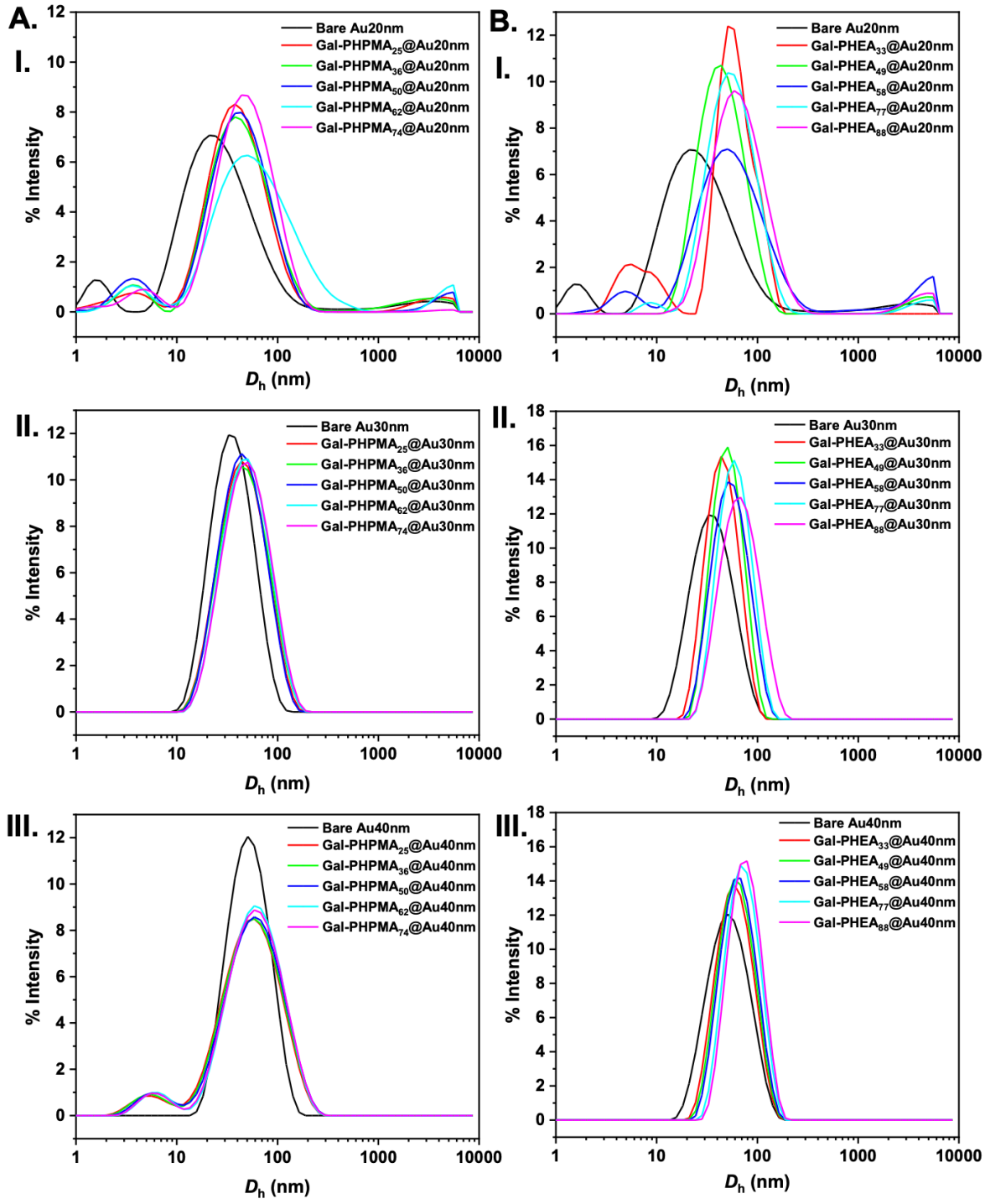

Figure S5. Intensity-weighted size distributions of (A) Gal-PHPMA and (B) Gal-PHEA functionalized gold nanoparticles with (I) 20, (II) 30 and (III) 40 nm gold nanoparticles.

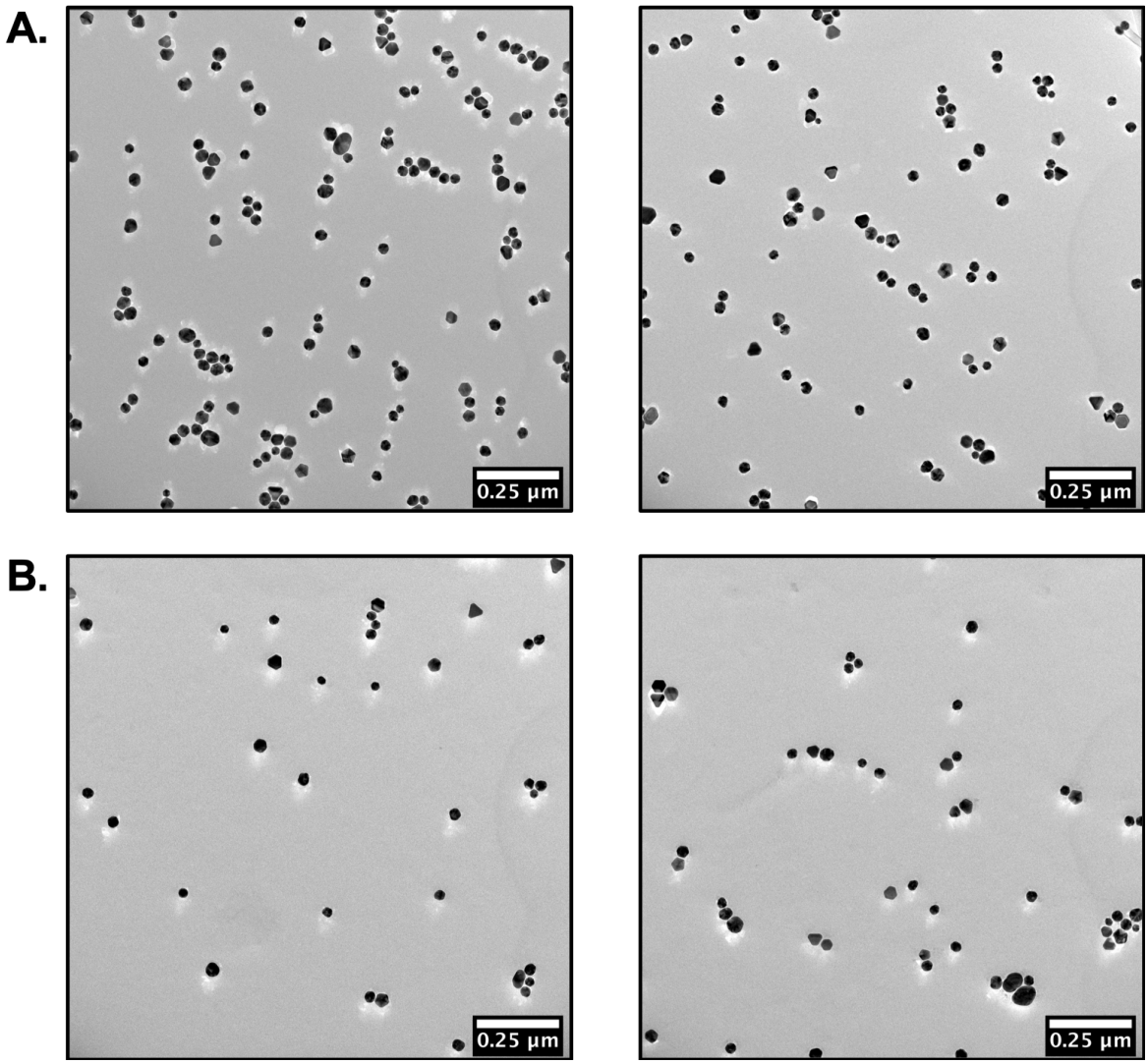

Figure S6. Representative dry-state TEM images of Gal-PHPMA$_{74}$@Au40nm and Gal-PHEA$_{77}$@Au40nm.

Table S1. Zeta-potential values measured from microelectrophoretic analysis at pH=7.

Particle	Zeta-Potential (mV)
Bare gold 20 nm	**-35.0 ± 1.5**
Gal-PHPMA$_{25}$@Au20	-37.1 ± 3.4
Gal-PHPMA$_{36}$@Au20	-29.9 ± 3.1
Gal-PHPMA$_{50}$@Au20	-27.5 ± 2.6
Gal-PHPMA$_{62}$@Au20	-27.5 ± 0.7
Gal-PHPMA$_{74}$@Au20	-27.2 ± 1.1
Gal-PHEA$_{33}$@Au20	-39.3 ± 4.2
Gal-PHEA$_{49}$@Au20	-33.7 ± 2.3
Gal-PHEA$_{58}$@Au20	-37.4 ± 2.0
Gal-PHEA$_{77}$@Au20	-40.8 ± 5.3
Gal-PHEA$_{88}$@Au20	-35.2 ± 1.7
Bare gold 30 nm	**-33.9 ± 1.0**
Gal-PHPMA$_{25}$@Au30	-26.0 ± 1.6
Gal-PHPMA$_{36}$@Au30	-27.7 ± 0.3
Gal-PHPMA$_{50}$@Au30	-29.5 ± 0.6
Gal-PHPMA$_{62}$@Au30	-21.8 ± 1.2
Gal-PHPMA$_{74}$@Au30	-20.3 ± 0.4
Gal-PHEA$_{33}$@Au30	-23.0 ± 1.5
Gal-PHEA$_{49}$@Au30	-25.0 ± 0.5
Gal-PHEA$_{58}$@Au30	-24.1 ± 1.1
Gal-PHEA$_{77}$@Au30	-21.6 ± 0.5
Gal-PHEA$_{88}$@Au30	-22.0 ± 3.4
Bare gold 40 nm	**-37.7 ± 3.1**
Gal-PHPMA$_{25}$@Au40	-26.6 ± 0.6
Gal-PHPMA$_{36}$@Au40	-20.2 ± 0.2
Gal-PHPMA$_{50}$@Au40	-22.1 ± 0.6
Gal-PHPMA$_{62}$@Au40	-21.1 ± 0.5
Gal-PHPMA$_{74}$@Au40	-19.5 ± 0.9
Gal-PHEA$_{33}$@Au40	-21.2 ± 3.8
Gal-PHEA$_{49}$@Au40	-31.3 ± 0.5
Gal-PHEA$_{58}$@Au40	-23.5 ± 3.3
Gal-PHEA$_{77}$@Au40	-20.5 ± 0.3
Gal-PHEA$_{88}$@Au40	-14.9 ± 0.9

Table S2. Elemental Compositions of PHEA functionalized particles including Au:N ratios

Particle		Particle Composition (%)				
AuNP (nm)	**PHEA DP**	**Au 4*f***	**C 1*s***	**N 1*s***	**O 1*s***	**Au 4*f*:N 1*s***
30	**33**	12.69	57.06	8.09	22.16	1:0.64
30	**49**	6.688	54.6	7.79	30.92	1:1.16
30	**58**	6.99	58.25	7.97	26.79	1:1.14
30	**77**	5.78	60.40	9.49	24.32	1:1.64
30	**88**	5.78	61.66	9.66	22.9	1:1.67

Table S3. Elemental Compositions of PHPMA functionalized particles including Au:N ratios

Particle		Particle Composition (%)				
AuNP (nm)	**PHPMA DP**	**Au 4*f***	**C 1*s***	**N 1*s***	**O 1*s***	**Au 4*f*:N 1*s***
30	**25**	22.00	53.01	5.59	19.40	1:0.25
30	**36**	20.21	54.97	6.56	18.26	1:0.32
30	**50**	14.37	58.16	6.40	21.07	1:0.45
30	**62**	12.28	58.31	6.15	23.26	1:0.50
30	**74**	12.86	60.10	6.42	20.62	1:0.50

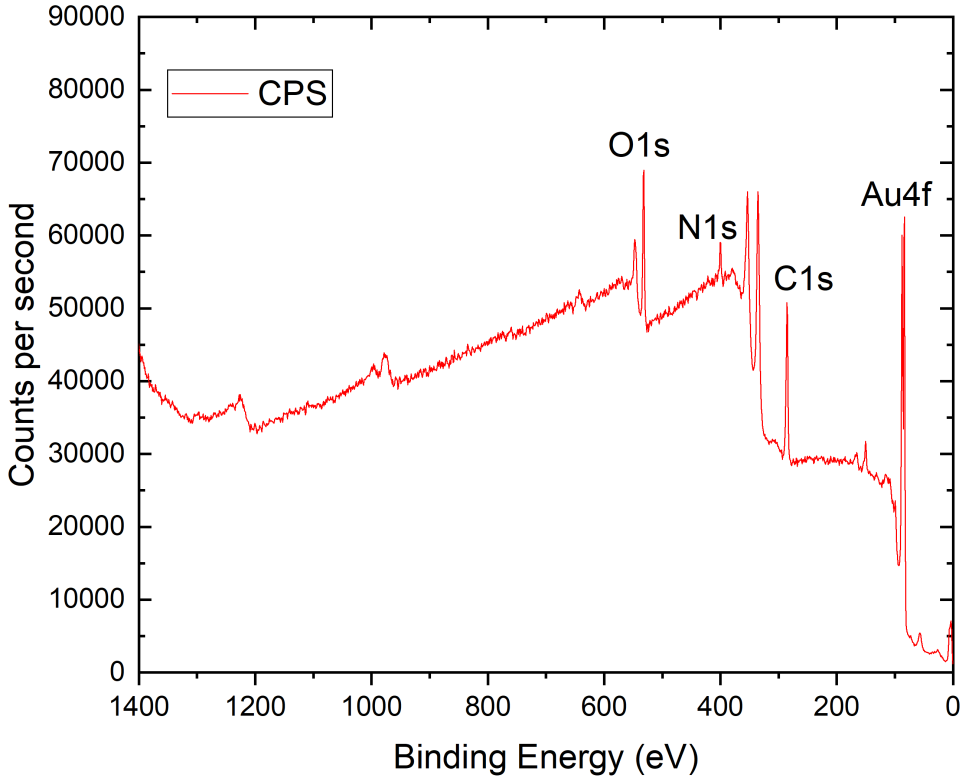

Figure S7. Representative XPS survey scan of Gal-PHPMA$_{50}$Au@AuNP$_{30}$.

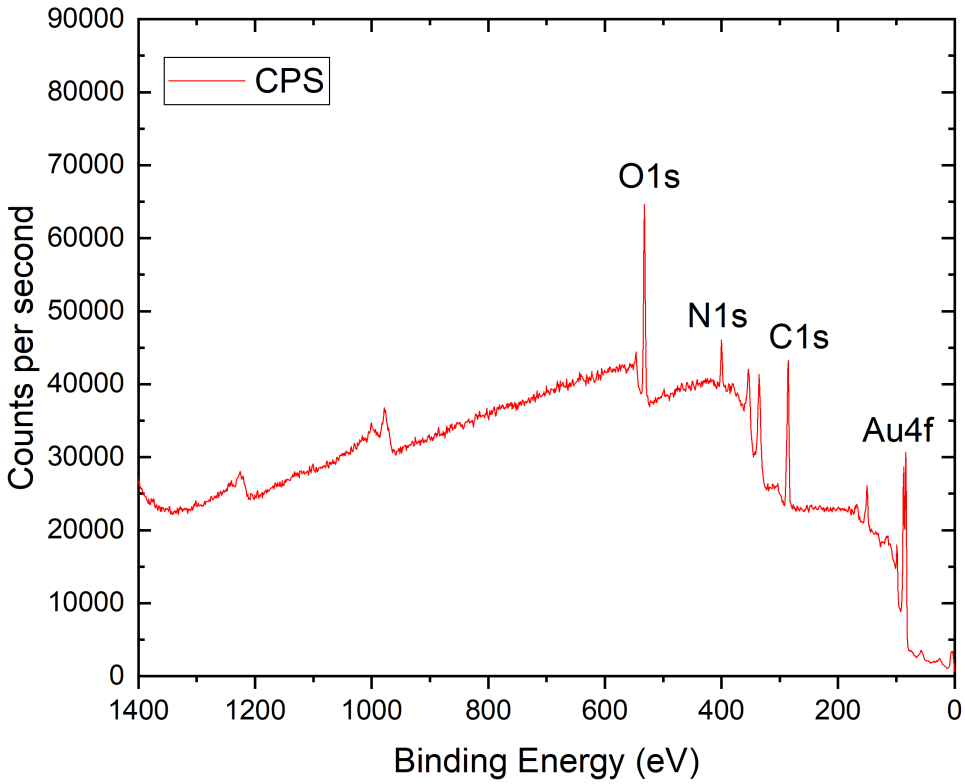

Figure S8. Representative XPS survey scan of Gal-PHEA$_{58}$Au@AuNP$_{30}$.

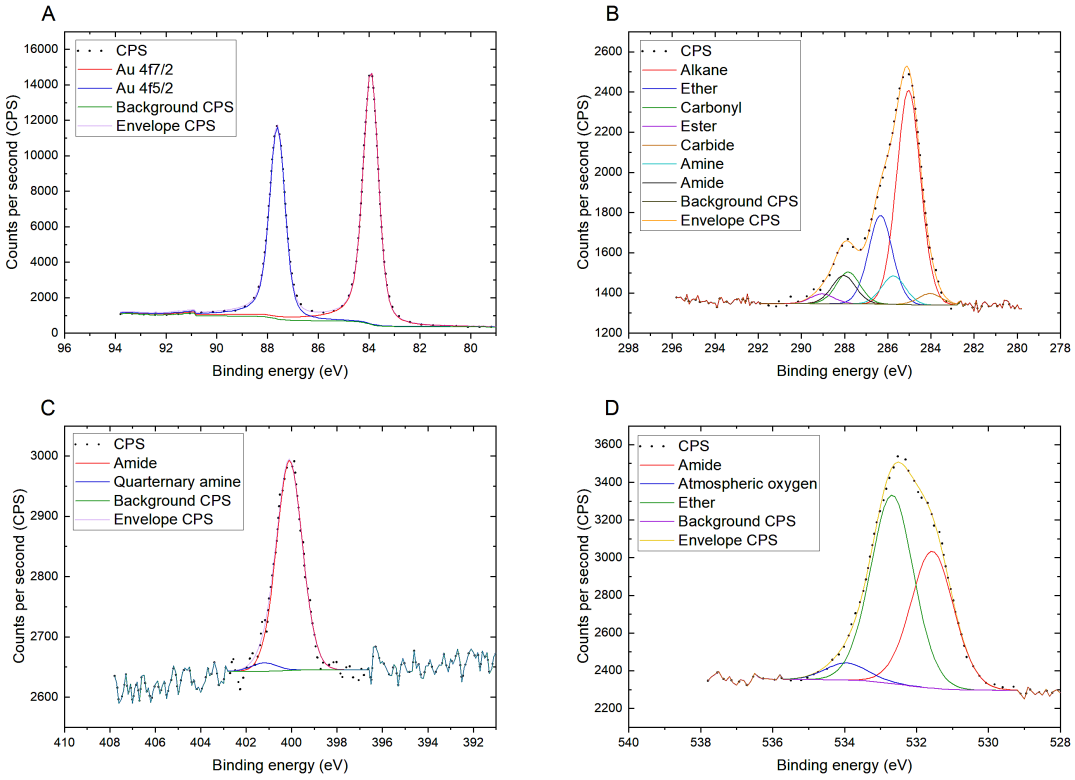

Figure S9. Representative XPS survey scans of Gal-PHPMA$_{25}$Au@AuNP$_{30}$ A) Au 4*f* B) C 1*s* C) N 1*s* D) O 1*s*.

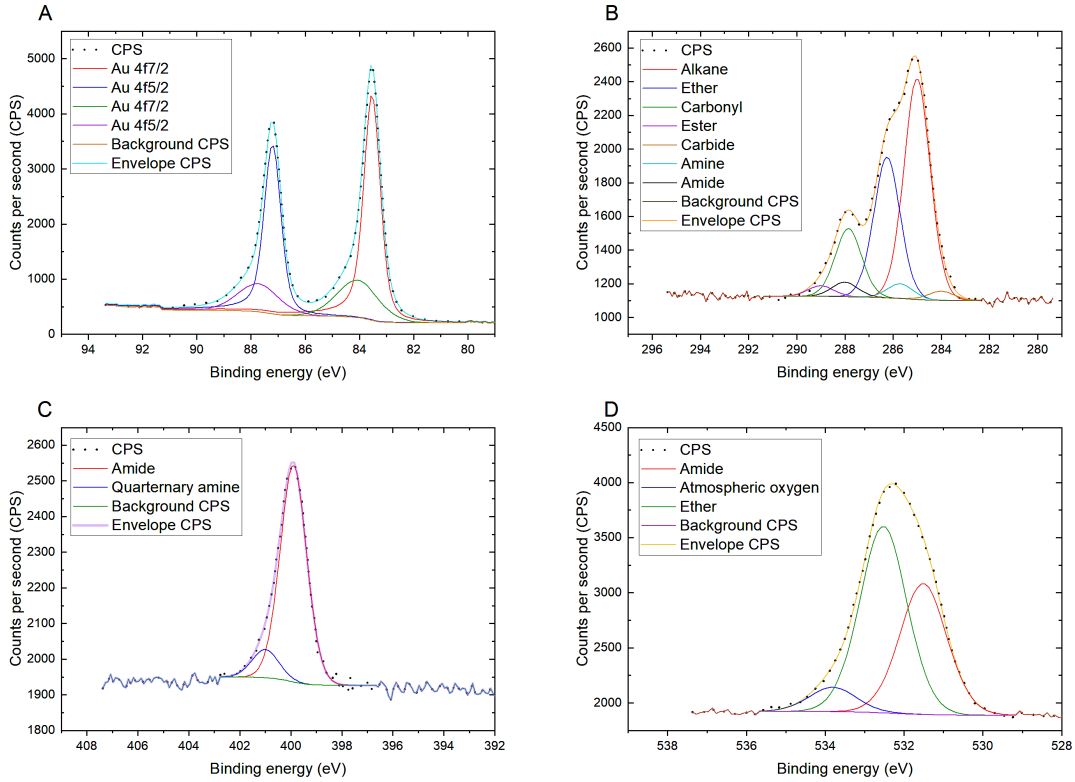

Figure S10. Representative XPS survey scan of Gal-PHEA$_{58}$Au@AuNP$_{30}$ for A) Au 4*f* B) C 1*s* C) N 1*s* D) O 1*s*.

Supplementary Characterization Data for Colloidal Stability and Lectin-Induced Aggregation Studies of Galactosylated-AuNPs

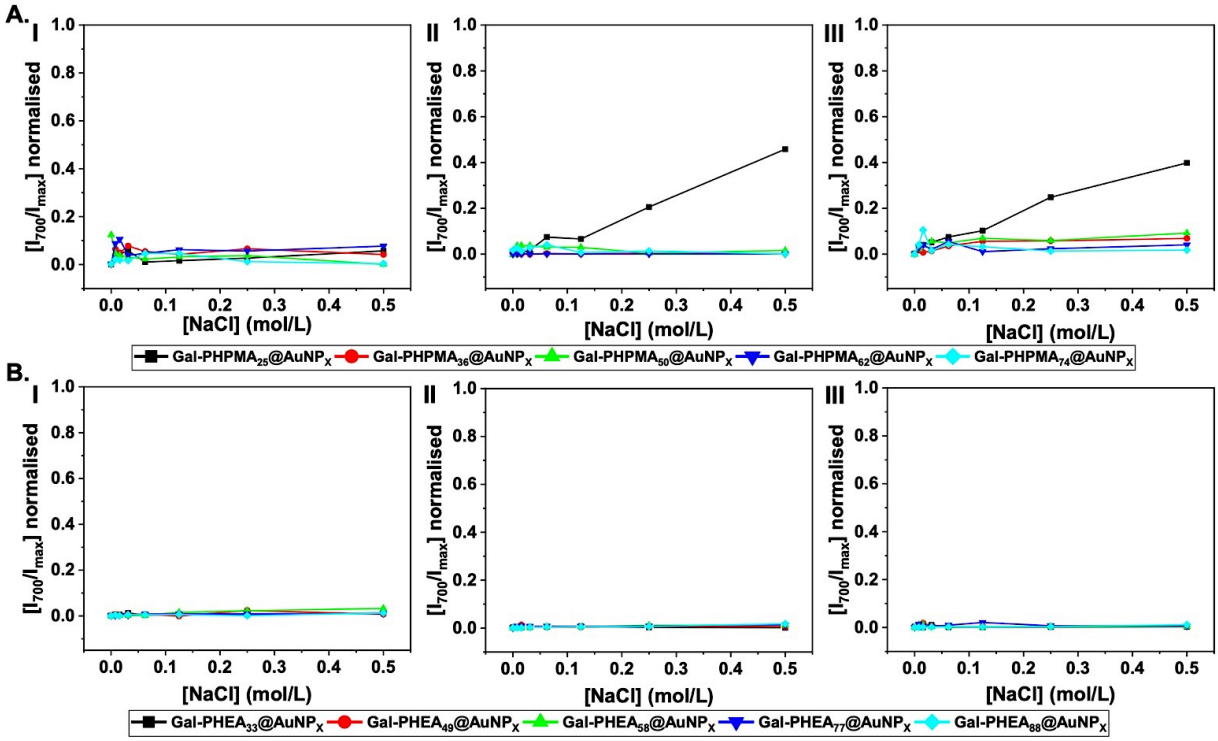

Figure S11. NaCl titration to determine saline stability of glycoparticles. (A) Gal-PHPMA and (B) Gal-PHEA coated AuNPs of (I) 20, (II) 30 and (III) 40 nm diameter. Plot of the ratio of the absorbance intensity at 700 nm and maximum intensity at 540 nm vs. NaCl concentration, after 30 minutes incubation at 37 °C.

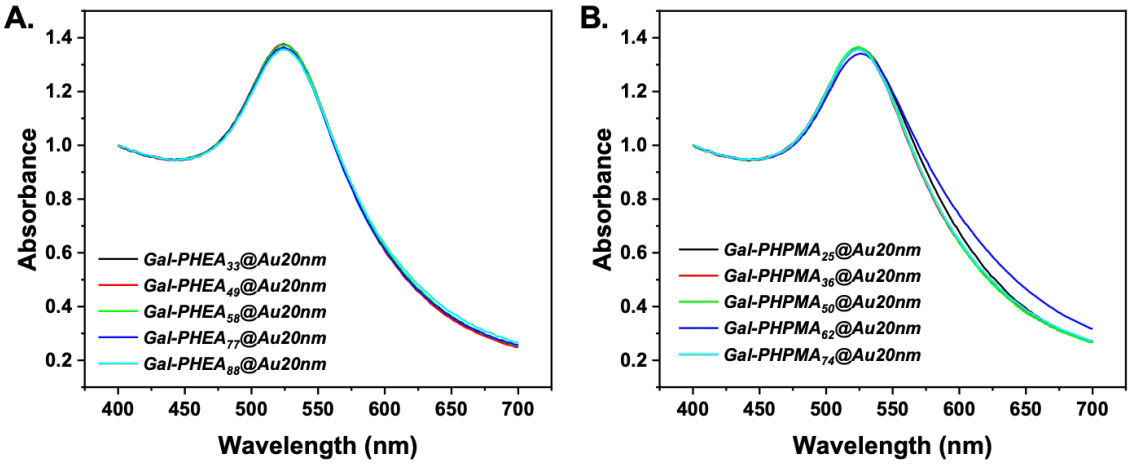

Figure S12. UV-vis spectra of Gal-PHPMA$_n$@AuNP$_{20nm}$ and Gal-PHEA$_x$@AuNP$_{20nm}$ nanoparticles (n=25, 36, 50, 62, 74 and x= 33, 49, 58, 77, 88 nm) upon incubation in buffer solution containing 10 mM HEPES, 0.15 M NaCl, 0.1 mM $CaCl_2$ and $MnCl_2$.

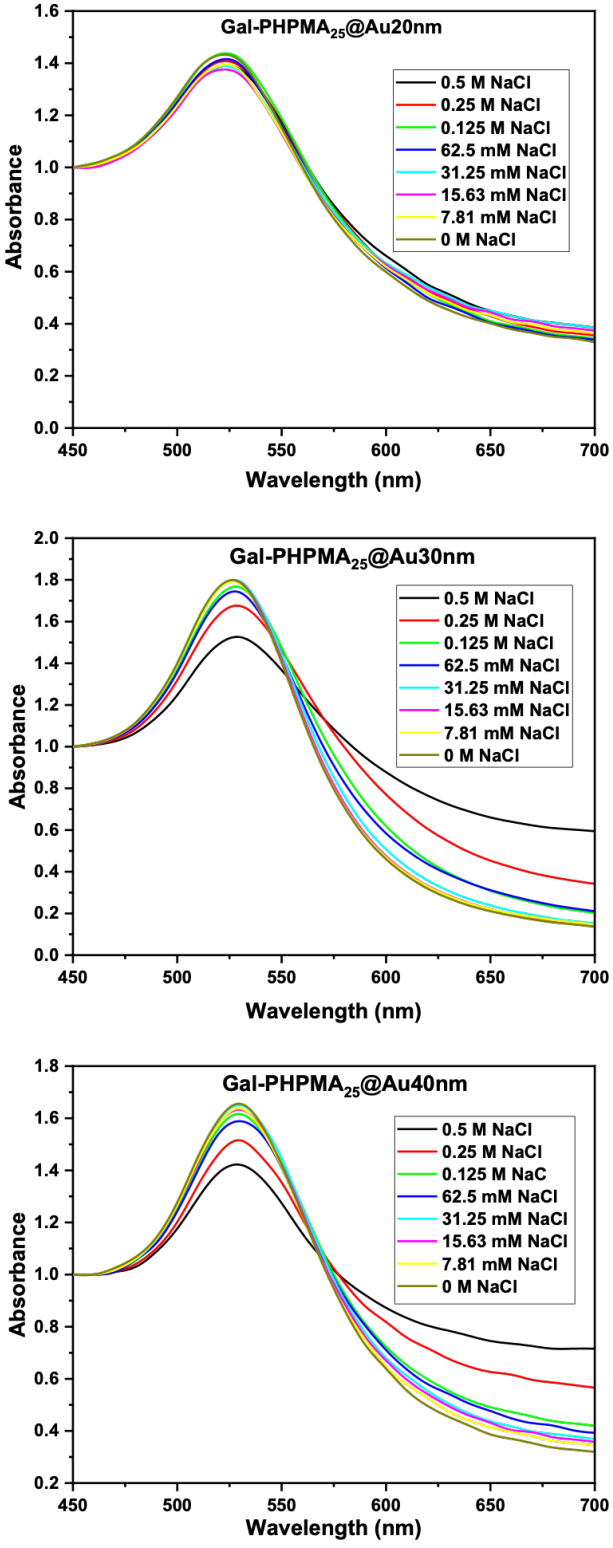

Figure S13. UV-vis spectra of Gal-PHPMA$_{25}$@AuNP$_X$ nanoparticles in response to different concentrations of NaCl (X= 20, 30 and 40 nm).

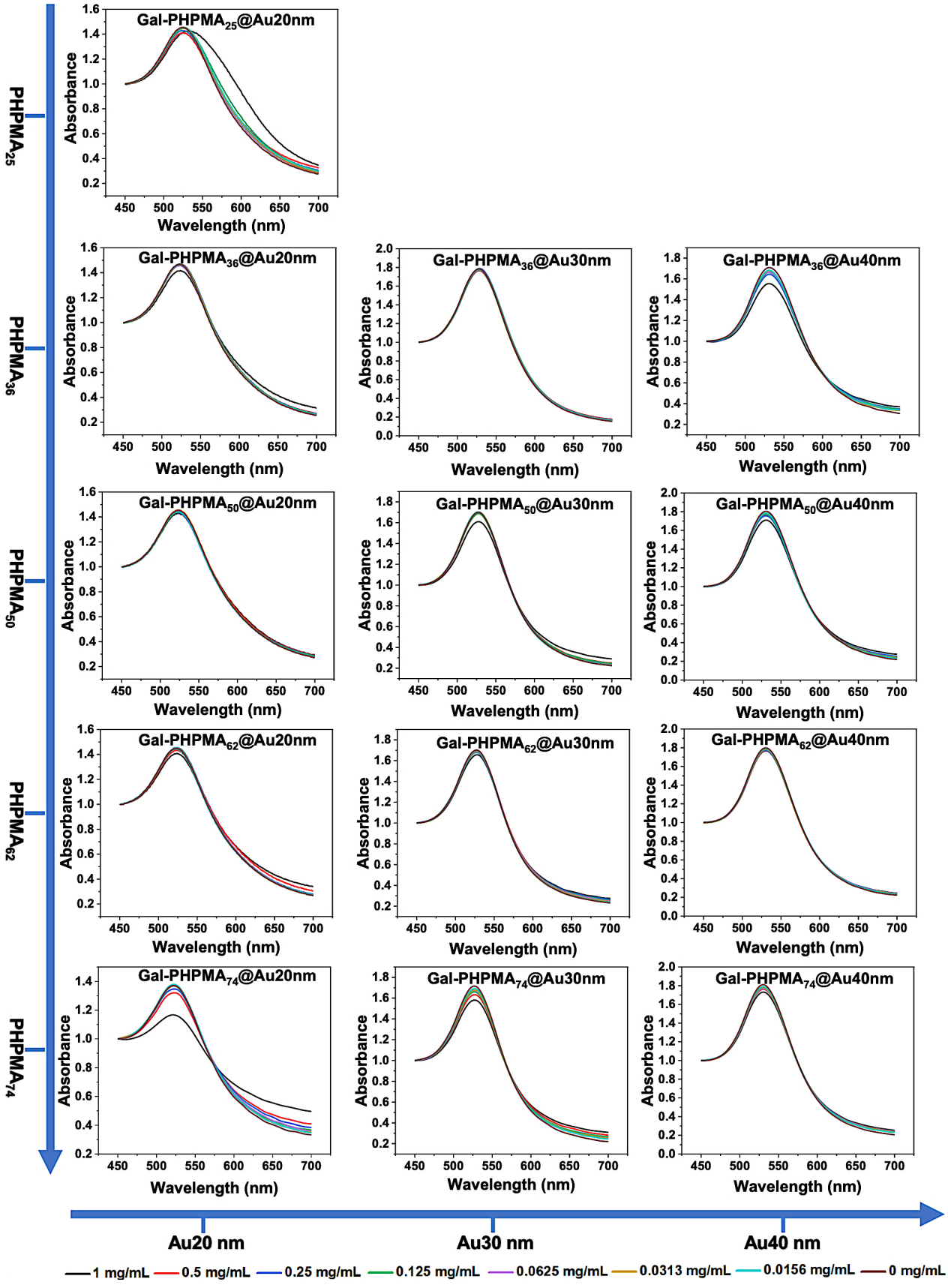

Figure S14. UV-vis spectra of Gal-PHPMA$_n$@AuNP$_X$ nanoparticles in response to SBA (n=25, 36, 50, 62, 74 and x= 20, 30, 40 nm).

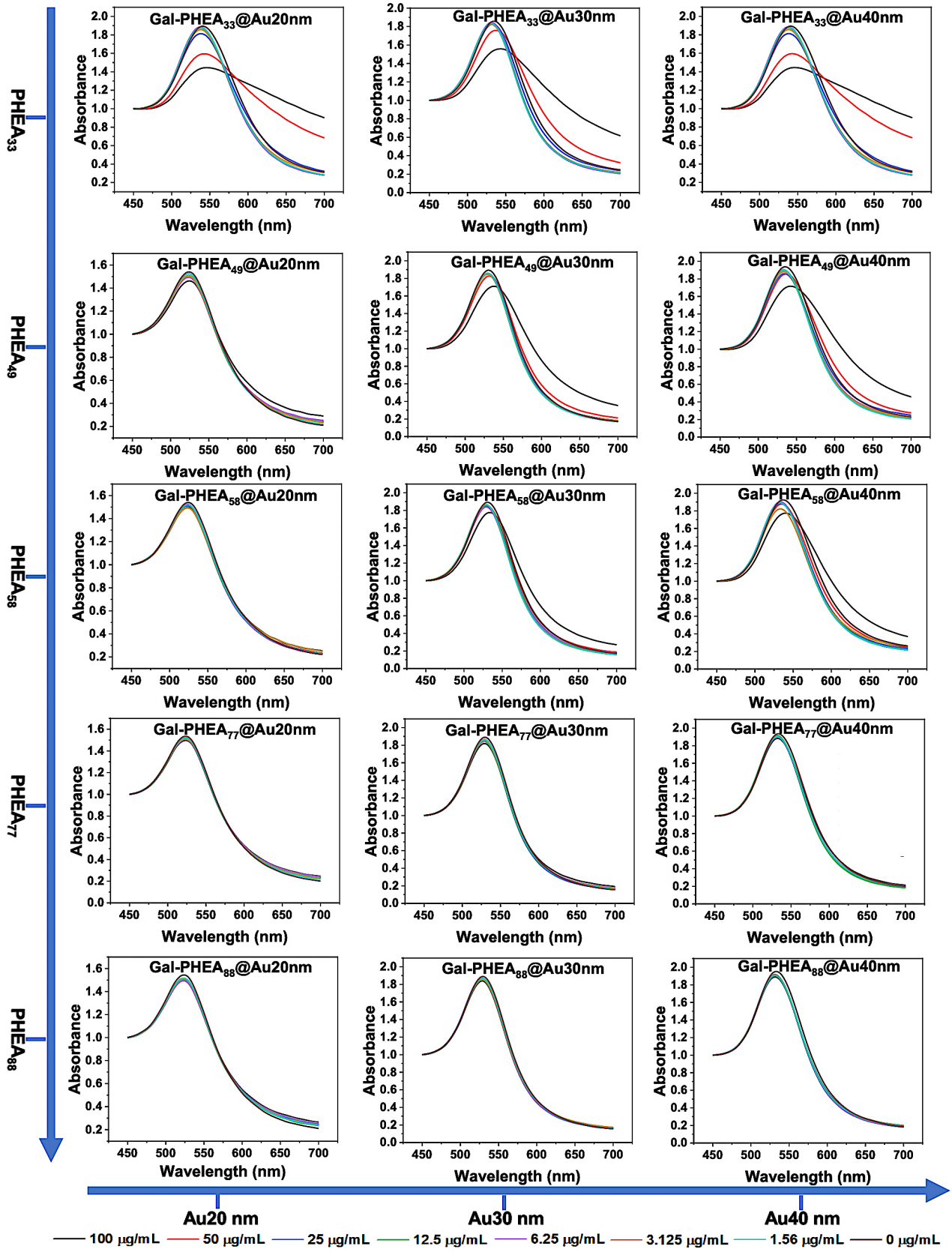

Figure S15. UV-vis spectra of Gal-PHEA$_n$@AuNP$_X$ nanoparticles in response to SBA (n=33, 49, 58, 77, 88 and x= 20, 30, 40 nm).

References

[1] N. G. Bastús, J. Comenge and V. Puntes, *Langmuir*, 2011, **27**, 11098–11105.